

Ignition and Oxidation of Core-Shell Al/Al₂O₃ Nanoparticles in Oxygen

Atmosphere: Insights from Molecular Dynamics Simulation

Qingzhao Chu¹, Baolu Shi^{1*}, Lijuan Liao^{2*}, Kai H Luo³, Ningfei Wang¹, Chenguang Huang²

¹ School of Aerospace Engineering, Beijing Institute of Technology, No.5 ZhongGuanCun South Street, Haidian, Beijing, 100081, CHINA

² Key Laboratory for Mechanics in Fluid Solid Coupling Systems, Institute of Mechanics, Chinese Academy of Sciences, No. 15 BeiSihuan West Road, Beijing, 100190, CHINA

³ Department of Mechanical Engineering, University College London, Torrington Place, London WC1E 7JE, United Kingdom

Corresponding Authors:

Baolu Shi^{1*} E-mail: smashingsky@hotmail.com, shibaolu@bit.edu.cn

Tel: +86-10-6891-3623

School of Aerospace Engineering, Beijing Institute of Technology, No.5 ZhongGuanCun South Street, Haidian, Beijing, 100081, CHINA

Lijuan Liao^{2*} Email: liaohuanxin@hotmail.com Tel: +86-10-8254-4291

Key Laboratory for Mechanics in Fluid Solid Coupling Systems, Institute of Mechanics, Chinese Academy of Sciences, No. 15 BeiSihuan West Road, Beijing, 100190, CHINA

Abstract

This study employed the reactive force field molecular dynamics to capture atomic-level heat and mass transfer and reaction processes of an aluminum nanoparticle (ANP) oxidizing in a high temperature and pressure oxygen atmosphere, revealing detailed mechanisms for oxidation of ANPs. Temporal variations of temperature, density, mean square displacement, atom consumption rate and heat release rate of ANP have been systematically examined. In addition, the effects of environment on ANP oxidation were also evaluated. The results show that ANP undergoes four stages of preheating, melting, fast Al core and moderate shell oxidations during the whole oxidation process. The Al core starts to melt from core-shell interface with outward diffusion of core Al atoms into the shell. Intense reaction occurs between shell O and core Al atoms around interface at the end of melting, leading to fast Al core oxidation. After complete oxidation of Al core, the oxide shell continues to react with ambient O atoms. Both the initial environmental temperature and the equivalent pressure significantly influence the preheating. Oppositely, the melting stage seems almost independent any of them. While the fast Al core oxidation presents more sensitivity to the ambient equivalent pressure.

1

2

3

4

5

6

7

8

9

10

11

12

13

14

15

16

17

18

19

20

21

22

23

24

25

26

27

28

29

30

31

32

33

34

35

36

37

38

39

40

41

42

1. Introduction

Owing to excellent energetic properties, such as ultra-high reactivity and high energy density, aluminum nanoparticles (ANPs) have been widely utilized in solid propellants and explosives^{1,2}. Despite wide-ranging existing and future applications, fundamental understanding of the ignition and oxidation mechanisms of ANPs is still lacking owing to extremely complex heat and mass transfer processes involving the Al core, passive alumina shell and environment.

Different oxidation mechanisms have been proposed from extensive studies, which are mainly summarized as three categories. Sundaram et al.^{3,4} pointed out that the oxidation rate of ANPs was controlled by chemical kinetics rather than mass diffusion, and the ANP oxidation scenarios mainly included eruptive oxidation, interfacial diffusion oxidation, and surface diffusion oxidation. For a ductile oxide layer or low heating rates, the ignition of ANPs was attributed to polymorphic transitions of shell and diffusion of aluminum and oxygen atoms across the oxide shell⁵. An experimental study at low heating rates (<10³ K/s) also reported that mass diffusion controlled oxidation kinetics⁶. As for a rigid oxide layer or fast heating rates, Levitas et al.⁷ proposed a melt-dispersion mechanism, in which mechanical breakdown of the oxide shell prompts dispersion of small Al clusters in the oxidizer, resulting in fast ignition. However, Li et al.⁸ reported that the shell of ANP did not break but just deformed over the oxidation process.

It is seen that so far whether the ANP oxidation rate is controlled by chemical kinetics^{3,4} or mass diffusion⁶ even melt-dispersion⁷ is still uncertain. Due to extremely short reaction time and particle aggregation during ANPs oxidation, it is still difficult to experimentally investigate detailed process of ANP combustion. Recently MD simulation has been employed to provide insights into oxidation mechanism of ANPs. In the study of Wang et al.⁹, the oxide shell was found to undergo catastrophic failure when the initial core temperature was above 6000 K. Moreover, they also examined the effects of oxide-shell structures on the oxidation of a laser flash heated ANP¹⁰. The results showed that ANP covered with an amorphous oxide-shell had much higher reactivity than that with a crystalline one.

1
2
3 Simulations by Henz et al.¹¹ demonstrated that the oxidation process was likely to occur by rapid
4 diffusion of aluminum cations driven by an induced electric field through the oxide shell. Zeng and
5 Cheng¹² performed MD simulations to study the atomic diffusion behaviors of core-shell ANPs during
6 heating process. They argued that the diffusivities of core Al atoms and shell O atoms at the core-shell
7 interfaces decreased by increasing the shell thickness after heating. The inward diffusion of shell O
8 atoms mainly contributed to the initial reaction at core-shell interface.
9
10

11 Most of these models focus on a certain stage, even though they are impressive and enlightening.
12 For example, in refs 9 and 10, the ANPs have been heated to above the melting temperature before the
13 initial oxidation. In refs 11 and 12, ANPs were in vacuum and the effects of surrounding oxygen atoms
14 were ignored. To the best of our knowledge, there are few, if any, systematic studies concerning the
15 whole process of ANP oxidation, while detailed insight into such a process will play a significant role
16 in improving understanding of ANP combustion. The current study adopts a model of preprocessed
17 core-shell ANP oxidizing in hot oxygen atmosphere, which is not only consistent with the real
18 combustion of ANP but also able to capture the atomic dynamics of ignition and oxidation process.
19
20

21 The objective of this work is to capture atomic-level heat and mass transfer and reaction processes
22 of an ANP oxidizing in an oxygen atmosphere; find an effective way that can directly depict the whole
23 process of ANP combustion and quantitatively identify different stages; and quantitatively evaluate the
24 effects of ambient environment on the ANP oxidation. Detailed insight into such a process is helpful
25 in improving control of ANP combustion.
26
27

2. Methods

2.1 Computational method

53 The reactive force field (ReaxFF)¹³ was adopted for the simulation of ANP oxidation. The general
54 expression for total energy used in the ReaxFF is shown in Eq. (1),
55
56

$$E_{\text{system}} = E_{\text{bond}} + E_{\text{over}} + E_{\text{under}} + E_{\text{lp}} + E_{\text{val}} + E_{\text{tors}} + E_{\text{vdWaals}} + E_{\text{coulomb}} \quad (1)$$

1
2
3 in which E_{bond} , E_{over} , E_{under} , E_{lp} , E_{val} , E_{tor} , E_{vdWaals} , and E_{coulomb} represent bond energy, over-coordination
4 energy penalty, under-coordination stability, lone pair energy, valence angle energy, torsion angle
5 energy, van der Waals energy, and coulomb energy, respectively. ReaxFF is a general bond-order based
6 force field, which is parameterized against quantum mechanics (QM) based training sets and able to
7 describe the bond formation and breaking which cannot be achieved by conventional MD methods¹⁴.
8
9 A comprehensive overview of ReaxFF development history can be found in a review literature by
10 Senftle et al.¹⁵. It has proved that the ReaxFF is more accurate than most of the semi-empirical methods;
11 furthermore, it is computationally much cheaper than the density functional theory (DFT), allowing
12 simulations in larger systems and longer physical time¹⁶. The ReaxFF has been developed for a wide
13 range of chemical systems such as hydrocarbon/oxygen¹⁷, silicon/silicon dioxide¹⁸, nickel/hydrocarbon
14 interactions¹⁹, titanium dioxide/water²⁰, aluminum/hydrocarbon²¹ and aluminum/ethanol interactions²².
15
16 In ref 15, various ReaxFF applications have also been examined to discuss the breadth of systems that
17 can be modelled with this method. It has been demonstrated that ReaxFF can successfully predict the
18 characteristics of chemically reactive systems. The Al-O ReaxFF parameters used in this paper have
19 been trained and validated by Hong et al.¹³.
20
21

2.2 Simulation details

1
2
3
4
5
6
7
8
9 The simulation mainly included two parts: (1) relaxation under the canonical ensemble (NVT) to
10 form a stable core-shell ANP structure, and (2) heat transfer and reaction between ANP and oxygen
11 under the micro-canonical ensemble (NVE). MD simulation, visualization and data post-processing
12 were conducted by LAMMPS²³, OVITO²⁴ and Matplotlib²⁵, respectively.
13
14

15 The initial structure of an ANP with an oxide shell was built according to Li's procedure⁸. A 6
16 nm-diameter Al core was cut from face-centered cubic (FCC) Al at 300 K. The amorphous oxide shell
17 was prepared by annealing the alpha-alumina, and then removing the outer and inner concentric parts
18 to obtain an oxide shell of 1 nm thickness. After combining the Al core and the oxide shell together,
19
20

the obtained ANP (Fig. 1 (a)) with radius of $R_p = 4$ nm was thermalized under NVT to form a stable core-shell interface. The particle temperature (T_p) was controlled at 300 K in NVT ensemble by Nose/Hoover thermostat with a time step (Δt) of 0.2 fs and a damping parameter of 20 fs. The sensitivities of the time step and the damping parameter have been discussed by the temporal variations of potential energy and T_p in Supporting Information (Fig. S1, $\Delta t = 0.1$ ²¹ and 0.2 fs; Fig. S3, a damping parameter of 20 fs). A time step as 0.2 fs and a damping parameter as 20 ps (100 times of Δt)²⁶ are sufficient to obtain reasonable results.

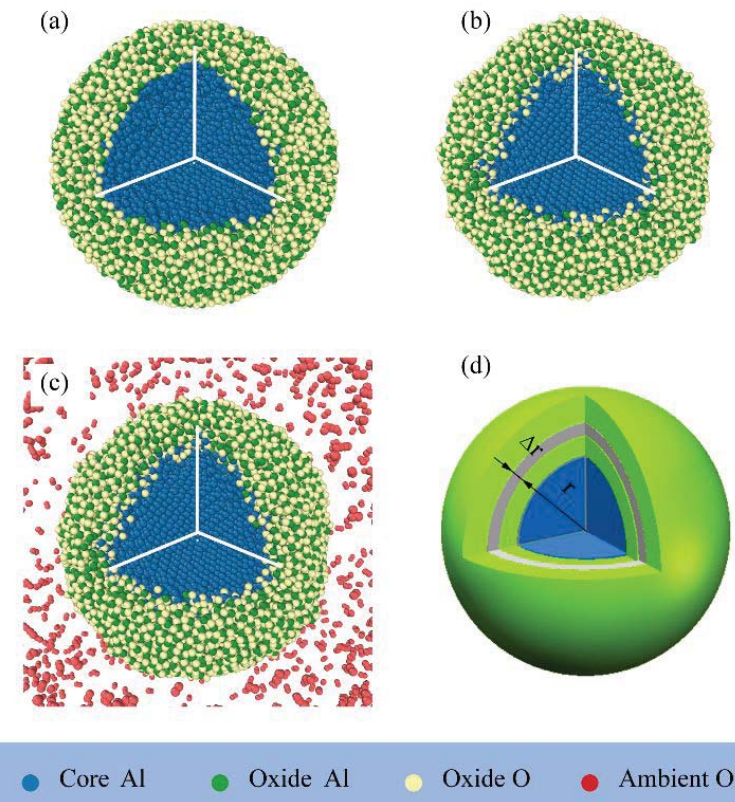


Figure 1 Snapshots of ANP at $t = 0$ ps (a) and $t = 160$ ps (b) during relaxation in NVT ensemble, initial configuration of ANP surrounded by oxygen molecules (c), and sketch of ANP structure (d). Property distribution within a thin spherical shell (grey shell in (d) with radius of r and thickness of Δr) was counted.

1

2

3 To obtain a reliable core-shell ANP model, the temporal variation of the particle potential energy
4 was examined as shown in Fig. 2. In this study, the solid lines are the average of three runs while the
5 translucent area indicates the error band. The potential energy changes abruptly during the first 20 ps,
6 which indicates that the initial structure of the ANP is unsteady. At $t = 120$ ps, the potential energy
7 varies slightly, and the core-shell interface becomes relatively stable. It should be noted that the curve
8 may continually decrease due to the very slow diffusion between Al and O atoms²⁷. The relative error
9 between the potential energy at $t = 140$ and 160 ps is less than 1.2%. The time point of $t = 160$ ps as
10 the end of relaxation is acceptable. The Al core radius (R_c) reduced to approximately 2 nm, and the
11 oxide shell thickness (δ) increased to 2 nm at the end of relaxation in NVT ensemble. The core-shell
12 interface was determined by the average radial position of 30 O atoms in the oxide shell nearest to the
13 ANP center. Similarly, the average radial position of 30 Al atoms in the oxide shell farthest from the
14 ANP center was adopted as the ANP surface.

15

16

17

18

19

20

21

22

23

24

25

26

27

28

29

30

31

32

33

34

35

36

37

38

39

40

41

42

43

44

45

46

47

48

49

50

51

52

53

54

55

56

57

58

59

60

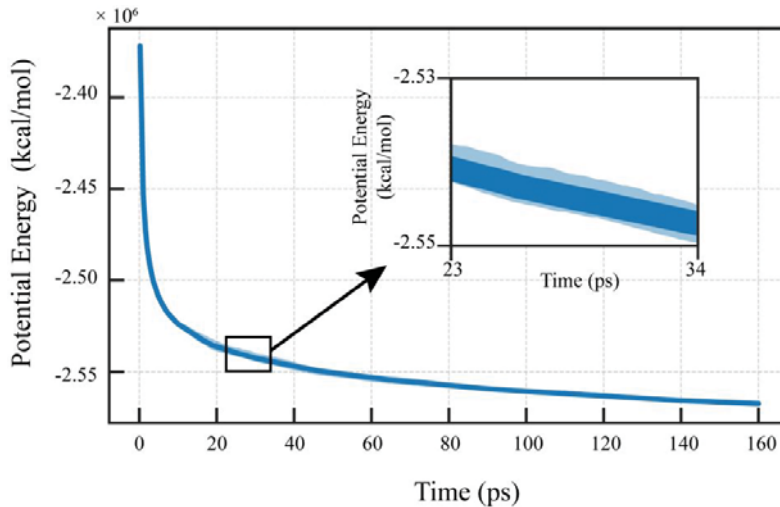


Figure 2 Temporal variation of ANP potential energy during relaxation in NVT ensemble.

Cases with different T_a and N_{O_2} were assigned in Table 1. Cases 1-3 with the same N_{O_2} were designed to evaluate T_a effect on the oxidation and reaction processes of ANP. The equivalent pressure of the environment was represented by the oxygen number in a given volume¹³. Accordingly, the influence of the initial pressure was investigated in cases 1, 4 and 5 at a given T_a .

Table 1 Case assignment in simulations.

ANP configuration	Case No.	T_a (K)	N_{O_2}
	1	2000	2700
$R_p = 4$ nm,	2	1000	2700
$R_c = 2$ nm,	3	3000	2700
$\delta = 2$ nm	4	2000	4041
	5	2000	5600

It is important to note that statistical noise is unavoidable in MD simulations, and previous ReaxFF studies indicated that to generate statistically significant results, multiple simulations need to be performed for each of the system^{17, 28}. To demonstrate the reproducibility of our results, each case was performed with three samples containing at least 25000 atoms.

1

2

3

4

5

6

7

8

9

10

11

12

13

14

15

16

17

18

19

20

21

22

23

24

25

26

27

28

29

30

31

32

33

34

35

36

37

38

39

40

41

42

43

44

45

46

47

48

49

50

51

52

53

54

55

56

57

58

59

60

3. Results and discussion

This section firstly examines the results of ANP oxidation for Case 1 in Table 1. It focuses on the overall time-evolutions of the ANP temperature, density and mean squared displacement (MSD), diffusion of atoms and variation of oxide structure. The results of five cases are then compared to clarify the effects of initial ambient temperature and equivalent pressure.

3.1 Overall time-evolution of ANP temperature and density

To visualize the reaction process, snapshots of the ANP central cross section are plotted. Thermodynamic properties such as temperature and density in the computational domain of the central cross section were calculated by averaging the properties in all cells. Figure 3 shows representative snapshots of temperature (a) and density (b) in the range of $t = 0$ -160 ps. Meanwhile, to make a quantitative analysis, the radial distribution of ANP temperature (a) and density (b) at corresponding time instants were calculated, as plotted in Fig. 4. The radial distribution was plotted by dividing the particle into different spherical shells. For the radial distribution of a property at a distance r from the centroid of the ANP, atoms in a spherical shell between r and $r+\Delta r$ were counted to calculate this property (see Fig. 1(d)). In this paper, Δr was selected as 2 Å.

At $t = 0$ ps, the initial temperature of the ANP is 300 K. The density of the Al core is about 2.7 g/cm³, and that of the oxide shell is nearly 3.5 g/cm³. The results agree well with the density of solid-state aluminum²⁹ and amorphous alumina³⁰ at 300 K. A low-density region (approximate 2.2 g/cm³) is observed near the core-shell interface, which may be caused by the reaction between the Al core and oxide shell. As time progresses, T_p gradually increases resulting from both heat transfer (between ANP and environment) and heat release from Al/O reaction. At $t = 60$ ps, the temperature of the Al core (T_c) increases to about 700 K, while that of the oxide shell (T_s) is a bit higher (~900 K), indicating the heat transfer process from the outer shell towards the center core. Owing to the small size of the ANP with ultra-low Biot number, the temperature distribution inside the Al core or oxide shell is almost uniform.

Meanwhile, the low-density region propagates toward the center of the Al core.

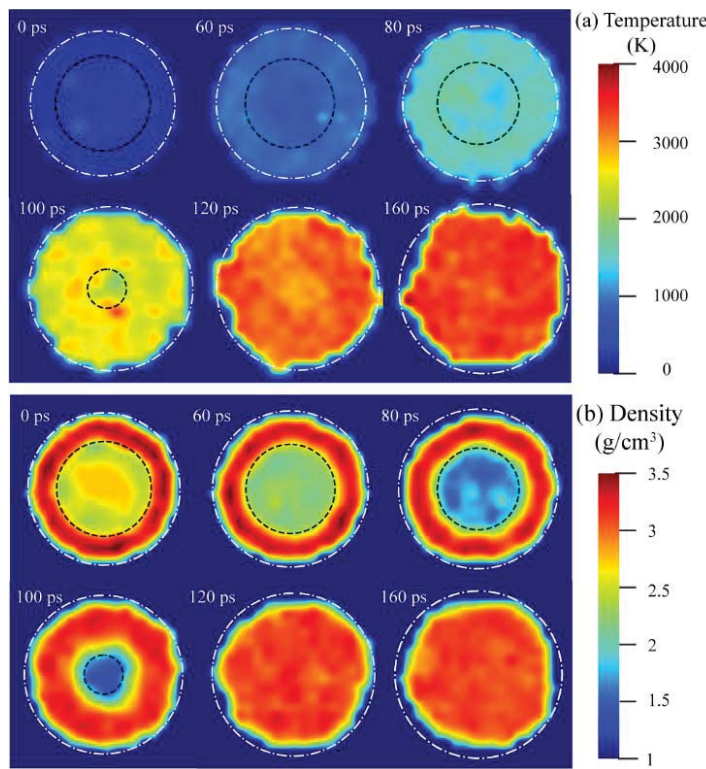


Figure 3 Representative snapshots of the cross sections of temperature (a) and density (b) distributions of ANP. The dash and dash-dot curves represent the core-shell interface and ANP surface, respectively.

At $t = 80$ ps, T_p rapidly rises to about 1500 K. The distribution of T_c becomes non-uniform, which is caused by local melting and oxidation and will be discussed in Section 3.2. The Al core density reduces to a value lower than 1.7 g/cm^3 , and the density of oxide shell also slightly decreases. The Al core shrinks, as indicated by the core-shell interface (blue dash lines in Fig. 4), while the particle surface expands outward (dash-dot lines). At $t = 100$ ps, T_p rises to about 2500 K. Near the core-shell interface, the temperature is slightly higher than those at other positions, which is probably attributed to exothermic Al/O reaction at the core-shell interface. The volumes of the Al core and oxide shell vary significantly, indicating the conversion of Al core to oxide shell. And the density distribution illustrates a large gradient around the core-shell interface. From $t = 120$ ps, the Al core is completely

1
2
3
4
5
6
7
8
9
10
11
12
13
14
15
16
17
18
19
20
21
22
23
24
25
26
27
28
29
30
31
32
33
34
35
36
37
38
39
40
41
42
43
44
45
46
47
48
49
50
51
52
53
54
55
56
57
58
59
60

oxidized; the distributions of temperature and density inside the ANP become almost uniform, both of which increase slightly with t . At $t = 160$ ps, the temperature of ANP reaches about 3200 K, and the density is nearly 3 g/cm^3 .

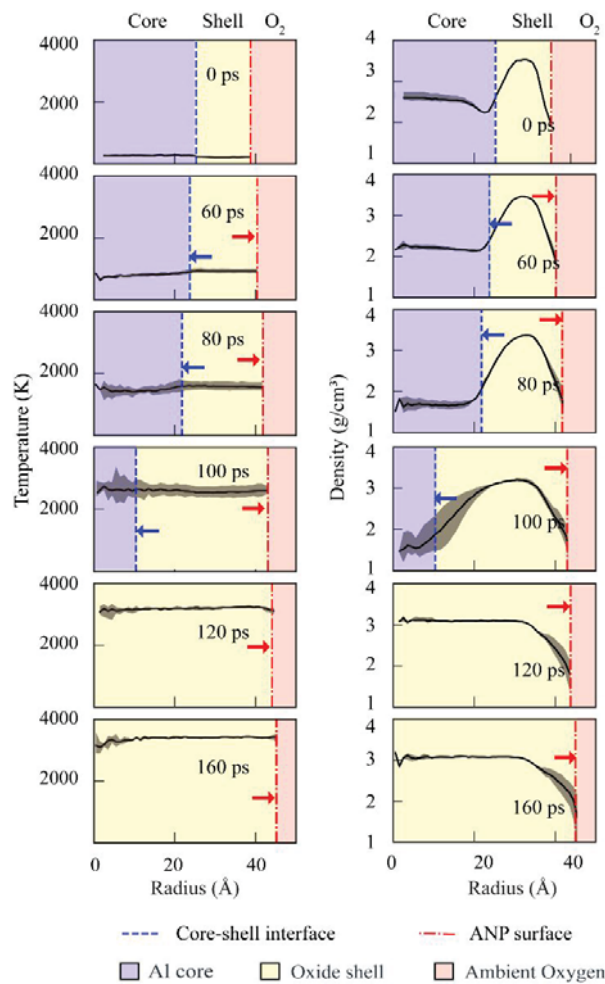


Figure 4 Radial distributions of ANP temperature (left) and density (right). The blue, yellow and red colors represent the Al core, oxide shell and ambient oxygen regions, respectively. The blue dash lines indicate the positions of core-shell interface, while the dash-dot lines represent the positions of ANP surface. The arrows show the moving directions of core-shell interface and ANP surface.

3.2 Phase transition and atomic diffusion

Generally, the melting point is defined as the temperature where sharp variations occur in the potential energy, translational-order parameter or radial distribution function profile^{31,32}. In the current study, the inflection point in MSD was adopted to predict the melting³³. This point indicates the transition from solid to liquid analogously to phase transition in macroscopy. In the following, the 'phase transition' represents the phenomenon similar to solid-to-liquid phase transition. MSD values of the Al core and oxide shell at every step were calculated, which represent the deviation of the atom position with respect to its reference position over time. Here the MSD during 10,000 steps was calculated and defined as MSD_{10000} .

In Fig. 5, MSD_{10000} and velocity distribution were computed in a cross section with a thickness of 6 Å. Their evolutions were integrated to characterize phase transition and atomic diffusion process. The average velocity of each atom can be determined by counting the displacement of each atom during an interval of 2 ps. The whole physical process is schematically depicted by the first row of Fig. 5, which experiences heat transfer, phase transition and atomic diffusion processes sequentially. Accordingly, four stages, that is, preheating, melting, fast Al core oxidation and moderate shell oxidation are qualitatively defined.

The Al core begins to melt at the core-shell interface from solid phase, as indicated by variation of MSD_{10000} (e.g., from $t = 34$ ps, 2nd row and 1st column to $t = 68$ ps, 2nd row and 2nd column in Fig. 5). Slight outward velocities indicate that the core Al atoms gradually diffuse into the oxide shell and react with shell O atoms, releasing heat to prompt further melting and oxidation. Outward diffusion velocities of core Al atoms significantly increase as the Al core approaching to the complete melting (e.g., $t = 88$ ps, 2nd row and 3rd column), resulting in intense core-shell reaction and a rapid shrinking of Al core. This exothermic reaction accelerates the melting of oxide shell (e.g., $t = 88$ ps, row 3-4 and

1

2

3

4 3rd column), which further prompts the core-shell reaction and inward diffusion of shell O atoms (e.g.,
5 $t = 88$ ps, 4th row and 3rd column). Zeng and Cheng¹² reported that the reaction initialization of core-
6 shell Al/Al₂O₃ nanoparticles mainly derived from the inward diffusion of oxygen atoms. We assumed
7 that both outward diffusion of core Al atoms and inward diffusion of shell O atoms contribute to the
8 oxidation. When the Al core has been completely oxidized, the ANP evolves as a nearly homogeneous
9 field (e.g., $t = 124$ ps, row 3-4 and 4th column).

10

11

12

13

14

15

16

17

18

19

20

21

22

23

24

25

26

27

28

29

30

31

32

33

34

35

36

37

38

39

40

The microstructural evolution of ANP in oxygen environment is illustrated in the bottom row of Fig. 5. During preheating, the ambient O atoms attach to the ANP surface. As the core melts, the core Al atoms obviously deviate from their equilibrated positions and diffuse into the oxide shell. As the core oxidation proceeds, shell O and ambient O atoms diffuse inward serially. The oxidation induced by shell O atoms plays a dominant role, which is different from the previously proposed oxidation mode (Al core react directly with environment O)^{34,35}. After the Al core has been completely oxidized, ambient O atoms continue diffusing into the shell to improve the oxidation level. Similar to Li's results⁸, shell of ANP does not break but just deforms over the oxidation process.

41

42

43

44

45

46

47

48

49

50

51

52

53

54

55

56

57

58

59

60

In order to examine the evolution of the ANP structure in more details, variations of the oxide shell size and its components were depicted by the ratio N_O/N_{Al} between O and Al atom number in Fig. 6(a). The shell thickness and N_O/N_{Al} in it hardly ever change until $t = 60$ ps approximately. The core-shell interface approaches to the ANP center in the following 20 ps. This trend remarkably accelerates across 80 ps until the interface diminishes, which indicates extreme outward diffusion of core Al atoms resulting in the decrease of N_O/N_{Al} . The diffusion of Al atoms in both core and shell was also examined by the number density, as indicated in Fig. 6(b). A severe decrease of core Al number density around $t = 80 - 100$ ps further confirms the outward diffusion of core Al atoms, as mentioned above. As $t > 100$ ps, the ANP evolves into oxide with homogeneous radial distribution gradually. At the end of

simulation, the radial distributions of N_O/N_{Al} and Al number density with tiny gradients indicate the dynamic equilibrium of atomic diffusion in the liquid phase oxide shell.

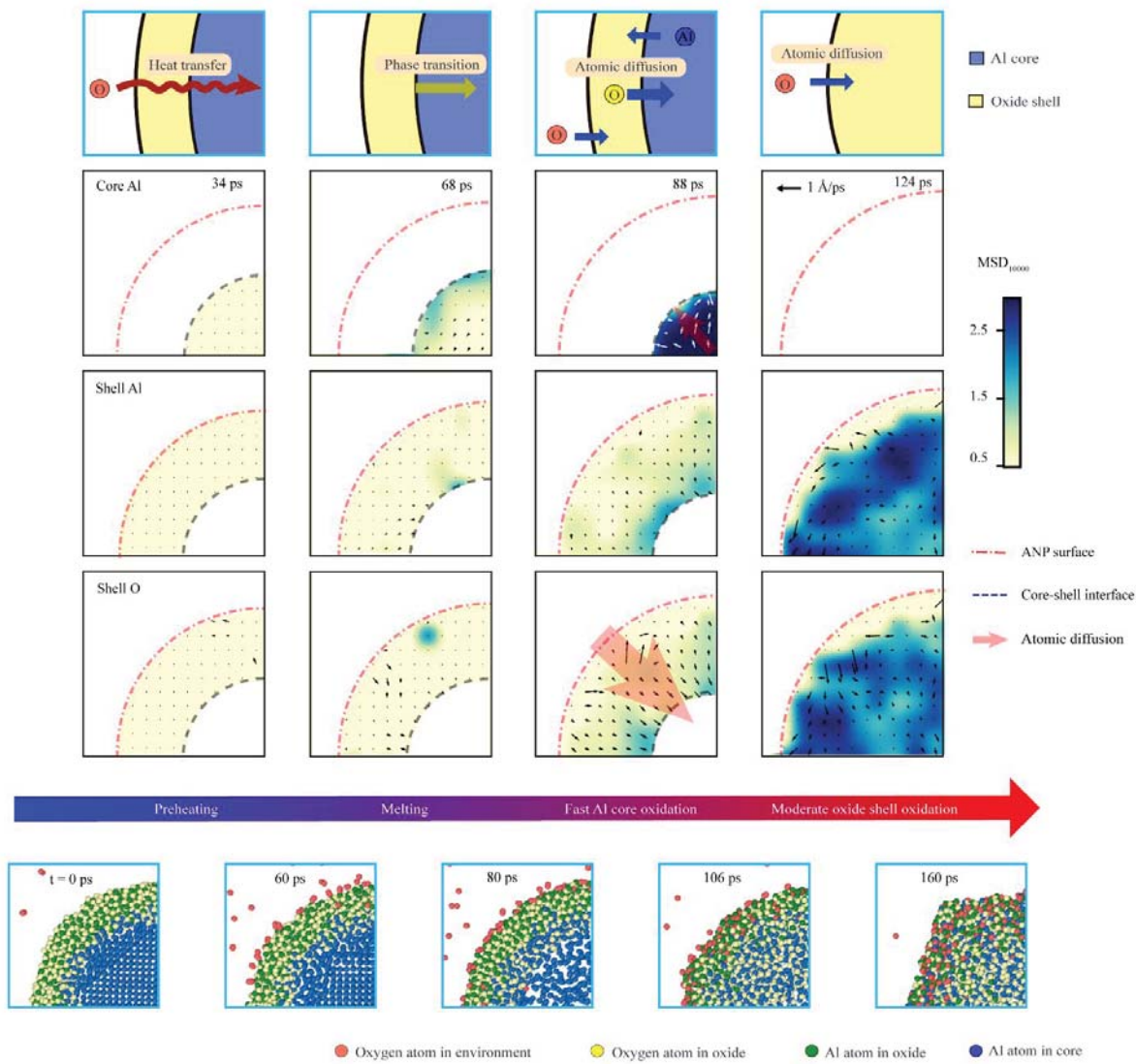


Figure 5 Schematic of heat and mass transfer processes (1st row), temporal MSD_{10000} contour and atomic diffusion vectors of core Al (2nd row), shell Al (3rd row) and shell O atoms (4th row), and snapshots of central cross section of ANP (bottom row).

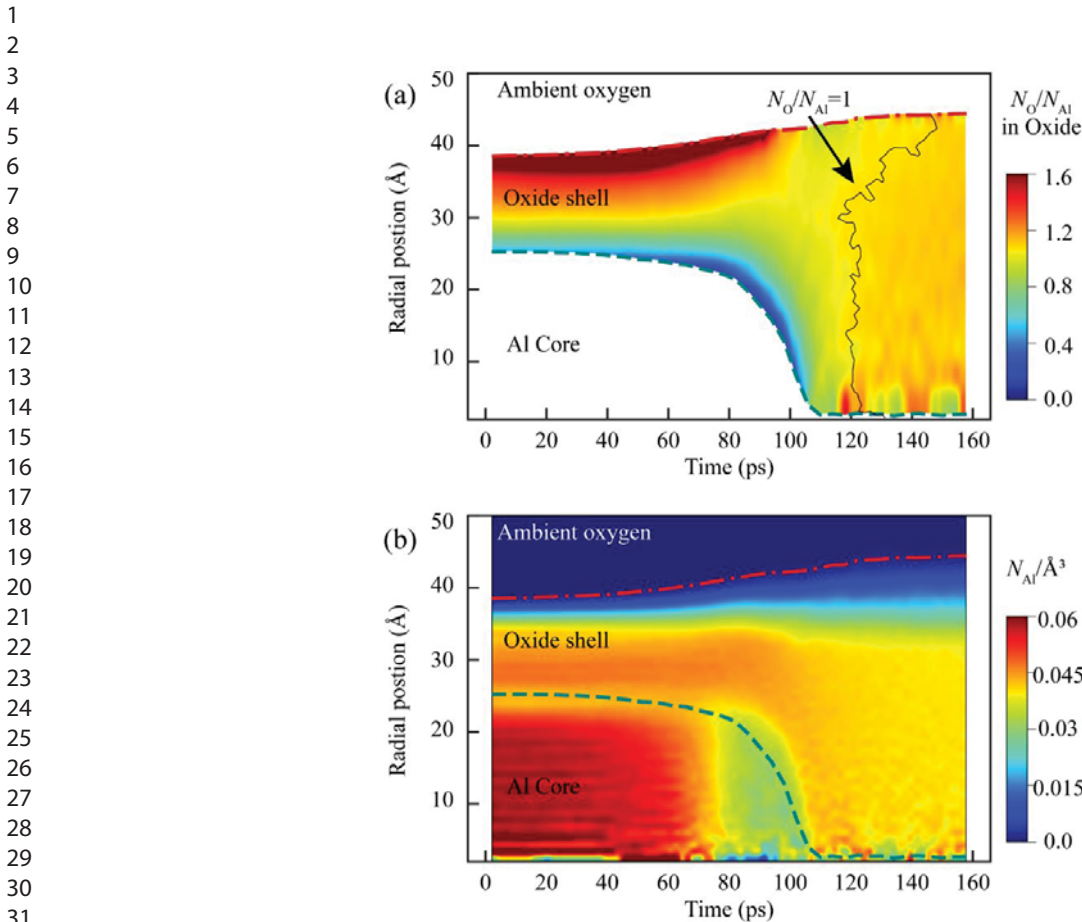


Figure 6 Evolution of ANP structures indicated by atoms distribution contours as well as distribution of O atom number to Al atom number ratio (N_O/N_{Al}) in oxide shell (a), and Al atom number density in the whole calculation domain (b). The dash and dash-dot curves are the core-shell interface and ANP surface, respectively.

3.3 Definition of four stages

In this section, the four stages as mentioned in Section 3.2 (Fig. 5) were quantitatively defined. The first inflection point (\blacktriangle) of MSD_{10000} of Al core indicates the transition from preheating to melting stage (Fig. 7(a)). The melting temperature of the core is 827 K on average in our simulations. According to the results of Puri et al.³⁶, the melting temperature for bare ANPs with a 5 nm diameter is 790 K, which is close to the current study.

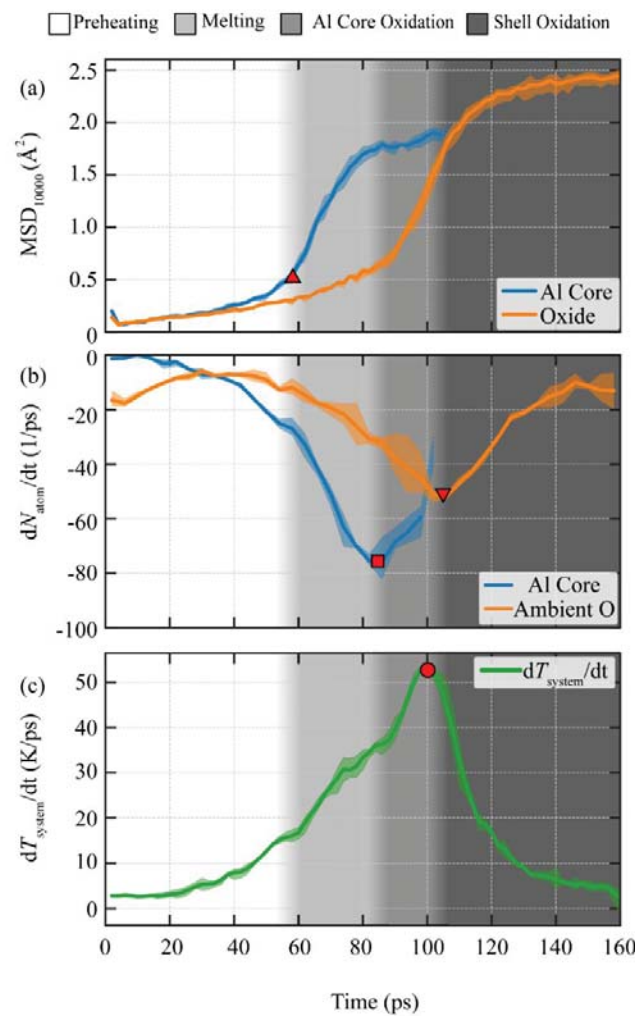


Figure 7 Temporal variations of global MSD_{1000} curves for Al core and oxide shell (a), consumption rates of core Al and surrounding O atoms (b), and derivative of system temperature (c). The preheating, melting, fast Al core oxidation and moderate oxide shell oxidation stages are indicated by different greyscales.

The overall time-evolutions of the core Al and ambient O atoms' consumption rates (dN_{atom}/dt , Fig. 7(b)), system temperature derivative (dT_{system}/dt , Fig. 7(c)) were also examined. Both of them are relatively low in preheating stage, indicating the weak Al/O reaction. As the Al core melts, dN_{Al}/dt significantly increases, prompting a rapid increase of dT_{system}/dt . The peak of dN_{Al}/dt (denoted by ■) is defined as the ignition of ANP in this study. Meanwhile, the Al core completely melts. After ignition,

dN_{Al}/dt is maintained at a high value until complete core oxidation (around $t = 106$ ps). At the same time, both dN_{O}/dt and dT_{system}/dt approach to their critical values (▼ and ●). In the moderate shell oxidation stage, both dN_{O}/dt and dT_{system}/dt gradually decreases, yielding a slow increase of temperature. Ambient O atoms continue diffusing into and reacting with the shell.

In summary, the ANP combustion process can be quantitatively divided into four stages determined by the dominant characteristic parameters in each stage. Different from other studies⁸⁻¹¹, the preheating and melting processes are analyzed comprehensively in this study. Furthermore, the oxidation process is divided into the fast oxidation stage of the Al core and the moderate oxidation stage of the oxide shell.

3.4 Effects of environmental conditions

In this section, the influences of initial ambient temperature and equivalent pressure on the four stages observed in this study were discussed. Five cases were designed as listed in Table 1. The ambient atoms may obtain higher kinetic energy as T_{a} increases (Case 2 → Case 1 → Case 3). While with increasing N_{O_2} (equivalent to environmental pressure, Case 1 → Case 4 → Case 5), the collision of ambient atoms with ANP atoms enhances.

For all cases, the ANPs were ignited successfully with the similar phenomena as Case 1. The durations for the preheating, melting and fast core oxidation stages were counted and plotted in Fig. 8. The elevation of T_{a} and N_{O_2} accelerates the preheating. However, the durations of melting stages in the designed cases vary slightly, which indicates that the effect of surrounding condition could be ignored. For the fast core oxidation, the duration is strongly affected by the equivalent pressure but not sensitive to the environmental temperature.

The energy (heat) transfer between the ANP and the environment is assumed to be accelerated in the preheating stage, owing to the enhancement of the collision probability as T_{a} and N_{O_2} increase.

The Al core melting proceeds from its outer surface to inner as the melting point front propagates inward, which is mainly governed by the thermal conductivity of the Al core at a given size, independent of T_a and N_{O_2} . For the fast core oxidation, the duration is strongly affected by N_{O_2} but not sensitive to T_a . Since at this stage, the temperature of the ANP is above 2500 K. The key factor of the fast Al core oxidation is atomic diffusion inside the oxide shell. The elevation of N_{O_2} increases the oxygen atom concentrations around the ANP surface, which can accelerate the inward diffusion of oxygen atoms and interfacial reaction.

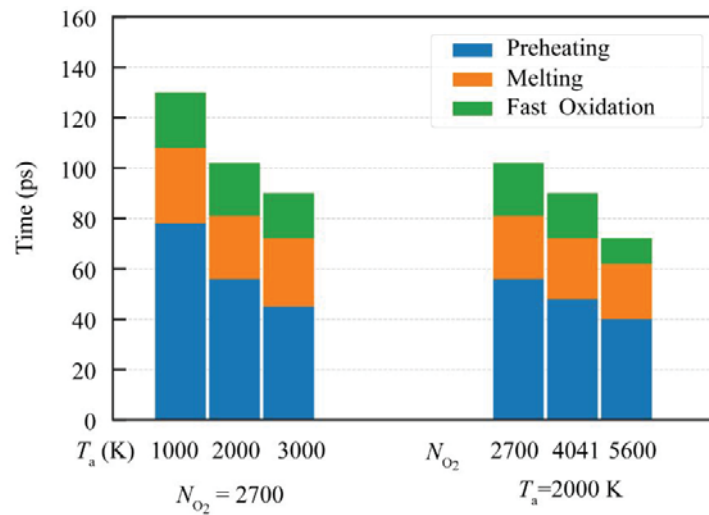


Figure 8 Durations of different stages under various T_a (left, with a constant $N_{O_2} = 2700$) and equivalent pressures (right, with a constant $T_a = 2000$ K).

4. Conclusions

The ReaxFF molecular dynamics has been employed to successfully capture the heat and mass transfer and reaction processes for aluminum nanoparticle (ANP) oxidation in a high temperature and pressure oxygen atmosphere. By examining the phase transition and atomic diffusion processes, atomistic oxidation mechanisms of the ANP are elucidated. Main conclusions are summarized as

1
2
3
4
5

follows:

6
7
8
9

(1) Oxidation of ANP experiences four stages as preheating, melting, fast Al core oxidation and moderate oxide shell oxidation sequentially.

10
11
12
13
14
15
16
17
18

(2) The Al core melting initiates at the core-shell interface, resulting in outward diffusion of core Al atoms. Reaction at the interfacial zone triggers ignition at the end of core melting, which further accelerates Al core oxidation. After complete oxidation of Al core, ambient O atoms continue reacting with the oxide shell.

19
20
21
22
23

(3) The outward diffusion of core Al atoms dominates in melting stage, while the inward diffusion of shell O enhances significantly in fast Al core oxidation stage.

24
25
26
27
28
29
30

(4) Higher initial ambient temperature and equivalent pressure shorten the preheating duration. The melting stage seems irrelevant to them. The equivalent pressure plays a significant role in the fast Al core oxidation stage positively.

31
32
33
34
35
36
37
38
39
40

The atomistic-level oxidation and reaction mechanisms provide an insight into physical understanding of ANP burning. This study also introduces an analysis and characterization method for size-effect examination in future, which is a key point in the fine controlling of energy release of ANP.

41
42

Supporting Information

43
44
45
46
47
48
49
50
51

The sensitivities of the time step and the damping parameter (Figure S1-3); the complete author list for ref 15 (at the end of Fig. S3); the evolution of the ANP cross section (Video).

52
53
54
55

Author information

56
57
58
59
60

Corresponding authors:

Baolu Shi (smashingsky@hotmail.com, shibaolu@bit.edu.cn) ORCID: 0000-0002-8638-4679

Lijuan Liao (liaohuanxin@hotmail.com) ORCID: 0000-0003-1753-6373

Acknowledgment

This work was supported by the Equipment Advance Research Field Foundation (Grant No. 61407200201) and National Natural Science Foundation of China (Grant No. 11672314 and No. 51676016). The computations were supported by the Computing Facility, Institute of Mechanics, Chinese Academy of Sciences, and Tianhe-2 National Supercomputer Center in Guangzhou. KHL's work was supported by the UK Engineering and Physical Sciences Research Council under the projects "UK Consortium on Mesoscale Engineering Sciences (UKCOMES)" (Grant Nos. EP/L00030X/1 and EP/R029598/1).

References

- (1) Maggi, F.; Bandera, A.; Galfetti, L.; De Luca, L. T.; Jackson, T. L. Efficient Solid Rocket Propulsion for Access to Space. *Acta Astronaut.* **2010**, *66*, 1563–1573.
- (2) Trunov, M. A.; Schoenitz, M.; Dreizin, E. L. Ignition of Aluminum Powders under Different Experimental Conditions. *Prop., Explos., Pyrotech.* **2005**, *30*, 36–43.
- (3) Sundaram, D. S.; Yang, V.; Zarko, V. E. Combustion of Nano Aluminum Particles (Review). *Combust. Explos. Shock Waves* **2015**, *51*, 173–196.
- (4) Sundaram, D. S.; Puri, P.; Yang, V. A General Theory of Ignition and Combustion of Nano- and Micron-Sized Aluminum Particles. *Combust. Flame* **2016**, *169*, 94–109.
- (5) Firmansyah, D. A.; Sullivan, K.; Lee, K. S.; Kim, Y. H.; Zahaf, R.; Zachariah, M. R.; Lee, D. Microstructural Behavior of the Alumina Shell and Aluminum Core before and after Melting of Aluminum Nanoparticles. *J. Phys. Chem. C* **2012**, *116*, 404–411.
- (6) Park, K.; Lee, D.; Rai, A.; Mukherjee, D.; Zachariah, M. R. Size-Resolved Kinetic

1
2
3 Measurements of Aluminum Nanoparticle Oxidation with Single Particle Mass Spectrometry.
4
5

6 *J. Phys. Chem. B* **2005**, *109*, 7290–7299.
7
8

9 (7) Levitas, V. I. Burn Time of Aluminum Nanoparticles: Strong Effect of the Heating Rate and
10
11 Melt-Dispersion Mechanism. *Combust. Flame* **2009**, *156*, 543–546.
12
13

14 (8) Li, Y.; Kalia, R. K.; Nakano, A.; Vashishta, P. Size Effect on the Oxidation of Aluminum
15
16 Nanoparticle : Multimillion-Atom Reactive Molecular Dynamics Simulations. *J. Appl. Phys.*
17
18 **2013**, *114*, 134312.
19
20

21 (9) Wang, W.; Clark, R.; Nakano, A.; Kalia, R. K.; Vashishta, P. Fast Reaction Mechanism of a
22
23 Core(Al)-Shell (Al_2O_3) Nanoparticle in Oxygen. *Appl. Phys. Lett.* **2009**, *95*, 1–4.
24
25

26 (10) Wang, W.; Clark, R.; Nakano, A.; Kalia, R. K.; Vashishta, P. Effects of Oxide-Shell Structures
27
28 on the Dynamics of Oxidation of Al Nanoparticles. *Appl. Phys. Lett.* **2010**, *96*, 2008–2011.
29
30

31 (11) Henz, B. J.; Hawa, T.; Zachariah, M. R. On the Role of Built-in Electric Fields on the Ignition
32
33 of Oxide Coated Nanoaluminum: Ion Mobility versus Fickian Diffusion. *J. Appl. Phys.* **2010**,
34
35 *107*, 024901.
36
37

38 (12) Zeng, H.; Cheng, X.; Zhang, C.; Lu, Z. Responses of Core–Shell Al/ Al_2O_3 Nanoparticles to
39
40 Heating: ReaxFF Molecular Dynamics Simulations. *J. Phys. Chem. C* **2018**, *122*, 9191–9197.
41
42

43 (13) Hong, S.; Van Duin, A. C. T. Molecular Dynamics Simulations of the Oxidation of Aluminum
44
45 Nanoparticles Using the ReaxFF Reactive Force Field. *J. Phys. Chem. C* **2015**, *119*, 17876–
46
47 17886.
48
49

50 (14) Van Duin, A. C. T.; Dasgupta, S.; Lorant, F.; Goddard, W. A. ReaxFF: A Reactive Force Field
51
52 for Hydrocarbons. *J. Phys. Chem. A* **2001**, *105*, 9396–9409.
53
54

55 (15) Senftle, T. P.; Hong, S.; Islam, M.; Kylasa, S. B.; Zheng, Y.; Shin, Y. K.; Junkermeier, C.;
56
57

1
2
3
4
5
6
7
8
9
10
11
12
13
14
15
16
17
18
19
20
21
22
23
24
25
26
27
28
29
30
31
32
33
34
35
36
37
38
39
40
41
42
43
44
45
46
47
48
49
50
51
52
53
54
55
56
57
58
59
60

Engel-herbert, R.; Janik, M. J.; Aktulga, H. M.; et al. The ReaxFF Reactive Force-field: Development, Applications and Future Directions. *Npj Comput. Mater.* **2016**, *2*, 15011.

(16) Mao, Q.; van Duin, A. C. T.; Luo, K. H. Investigation of Methane Oxidation by Palladium-Based Catalyst via ReaxFF Molecular Dynamics Simulation. *Proc. Combust. Inst.* **2017**, *36*, 4339–4346.

(17) Chenoweth, K.; van Duin, A. C. T.; Goddard, W. A. ReaxFF Reactive Force Field for Molecular Dynamics Simulations of Hydrocarbon Oxidation. *J. Phys. Chem. A* **2008**, *112*, 1040–1053.

(18) van Duin, A. C. T.; Strachan, A.; Stewman, S.; Zhang, Q.; Xu, X.; Goddard, W. A. ReaxFF_{SiO} Reactive Force Field for Silicon and Silicon Oxide Systems. *J. Phys. Chem. A* **2003**, *107*, 3803–3811.

(19) Mueller, J. E.; van Duin, A. C. T.; Goddard, W. A. Development and Validation of ReaxFF Reactive Force Field for Hydrocarbon Chemistry Catalyzed by Nickel. *J. Phys. Chem. C* **2010**, *114*, 4939–4949.

(20) Kim, S. Y.; Kumar, N.; Persson, P.; Sofo, J.; Van Duin, A. C. T.; Kubicki, J. D. Development of a ReaxFF Reactive Force Field for Titanium Dioxide/Water Systems. *Langmuir* **2013**, *29*, 7838–7846.

(21) Hong, S.; Van Duin, A. C. T. Atomistic-Scale Analysis of Carbon Coating and Its Effect on the Oxidation of Aluminum Nanoparticles by ReaxFF-Molecular Dynamics Simulations. *J. Phys. Chem. C* **2016**, *120*, 9464–9474.

(22) Zhang, Y. R.; van Duin, A. C. T.; Luo, K. H. Investigation of Ethanol Oxidation over Aluminum Nanoparticle Using ReaxFF Molecular Dynamics Simulation. *Fuel* **2018**, *234*, 94–100.

(23) Plimpton, S. Fast Parallel Algorithms for Short-Range Molecular Dynamics. *J. Comput. Phys.*

1
2
3
4 **1995**, *117*, 1–19.
5
6 (24) Stukowski, A. Visualization and Analysis of Atomistic Simulation Data with OVITO-the Open
7 Visualization Tool. *Model. Simul. Mater. Sci. Eng.* **2010**, *18*, 015012.
8
9 (25) Hunter, J. D. Matplotlib: A 2D Graphics Environment. *Comput. Sci. Eng.* **2007**, *9*, 99–104.
10
11 (26) Plimpton, S.; Thompson, A.; Crozier, P. LAMMPS Users Manual (Aug 2017).
12
13
14 <https://lammps.sandia.gov/doc/Manual.pdf>.
15
16
17 (27) Chakraborty, P.; Zachariah, M. R. Do Nanoenergetic Particles Remain Nano-Sized during
18 Combustion? *Combust. Flame* **2014**, *161*, 1408–1416.
19
20
21 (28) Castro-Marcano, F.; Kamat, A. M.; Russo, M. F.; van Duin, A. C. T.; Mathews, J. P. Combustion
22 of an Illinois No. 6 Coal Char Simulated Using an Atomistic Char Representation and the
23
24 ReaxFF Reactive Force Field. *Combust. Flame* **2012**, *159*, 1272–1285.
25
26
27
28
29
30 (29) Hatch, J. E. *Aluminum: Properties and Physical Metallurgy*; American Society for Metals:
31
32 Metals Park, Ohio, USA, 1984.
33
34
35
36
37 (30) Adiga, S. P.; Zapol, P.; Curtiss, L. A. Atomistic Simulations of Amorphous Alumina Surfaces.
38
39 *Phy. Rev. B* **2006**, *74*, 064204.
40
41
42 (31) Cheng, X. L.; Zhang, J. P.; Zhang, H.; Zhao, F. Molecular Dynamics Simulations on the Melting,
43 Crystallization, and Energetic Reaction Behaviors of Al/Cu Core-Shell Nanoparticles. *J. Appl.*
44
45 *Phys.* **2013**, *114*, 084310.
46
47
48
49
50 (32) Alavi, S.; Thompson, D. L. Molecular Dynamics Simulations of the Melting of Aluminum
51 Nanoparticles. *J. Phys. Chem. A* **2006**, *110*, 1518–1523.
52
53
54 (33) Davoodi, J.; Dadashi, S.; Yarifard, M. Molecular Dynamics Simulations of the Melting of Al–
55 Ni Nanowires. *Philos. Mag.* **2016**, *96*, 2300–2310.
56
57
58
59
60

1
2
3
4 (34) Zhang, S.; Dreizin, E. L. Reaction Interface for Heterogeneous Oxidation of Aluminum Powders.
5
6 *J. Phys. Chem. C* **2013**, *117*, 14025–14031.
7
8

9 (35) Nie, H.; Zhang, S.; Schoenitz, M.; Dreizin, E. L. Reaction Interface between Aluminum and
10 Water. *Int. J. Hydrogen Energy* **2013**, *38*, 11222–11232.
11
12

13 (36) Puri, P.; Yang, V. Effect of Particle Size on Melting of Aluminum at Nano Scales. *J. Phys. Chem.*
14 *C* **2007**, *111*, 11776–11783.
15
16
17
18
19
20
21
22
23
24
25
26
27
28
29
30
31
32
33
34
35
36
37
38
39
40
41
42
43
44
45
46
47
48
49
50
51
52
53
54
55
56
57
58
59
60

